JOURNAL OF MATERIALS SCIENCE **36** (2001) 93–98

Structure and properties of stacking faulted A15 tungsten thin films

Y. G. SHEN*, Y. W. MAI
Centre for Advanced Materials Technology (CAMT), Department of Mechanical and Mechatronic Engineering, University of Sydney, NSW 2006, Australia
E-mail: yshen@mech.eng.usyd.edu.au

A combination of energy-filtered electron diffraction, x-ray photoelectron spectroscopy, electron energy-loss spectroscopy, field-emission scanning electron microscopy, and x- ray diffraction are used to establish that oxygen impurities incorporated in the tungsten films prepared by magnetron sputtering play a dominant role in the formation of the stacking faulted A15 W structure. Energy-filtered electron diffraction data collected from A15 films were Fourier transformed to a reduced density function (RDF), which is compared to theoretical calculations based on several possible structural models. By using a reliability *R*-factor analysis the A15 W structure has been determined to be a mixed phase consisting of ordered and stacking faulted W_3W structures. The effect of oxygen in stabilizing the stacking faulted A15 structure was also elucidated by *in situ* anneal and discussed on the basis of structural and thermodynamic stability. © *2001 Kluwer Academic Publishers*

1. Introduction

The stable structure of sputtered tungsten thin films is body-centred-cubic (bcc α-W). However, a metastable form of A15 tungsten (β-W) has long been reported. The nature and properties of A15 W films have been studied extensively by many research groups [1–15]. These investigations have mainly focused on electrical resistivity, density, phase transition, surface morphology, microstructure, and residual stress as a function of processing conditions. However, structural details of A15 W films are not yet well characterized or understood because of the difficulty of specimen preparation and structural analysis. In particular, observations in transmission electron microscopy (TEM) and analysis by x-ray diffraction (XRD) did not give structural details due to large uncertainties involved in diffraction and spectroscopic measurements and to different interpretations of experiments. In addition, complications caused by the simultaneous presence of the forbidden reflections in the A15 W films observed in transmission electron diffraction (TED) have not been resolved yet [10–15]. It is far from clear as to how oxygen impurities play a key role in forming and stabilizing the A15 structure in W thin films.

In this paper, structural details of A15 W films prepared by magnetron sputtering are presented, in which some new features not reported in previous studies of this system have been revealed. Oxygen impurities were analyzed by x-ray photoelectron spectroscopy (XPS) and electron energy-loss spectroscopy (EELS). The structure was probed at the atomic level for the first time using energy-filtered electron diffraction (EFED) with a reduced density function (RDF) analysis. By using a reliability (R) factor analysis to compare the experimental and simulated RDF distributions, the stacking faulted A15 structure has been determined. The role of oxygen impurities in stabilizing the A15 phase was also elucidated by *in situ* anneal using EELS, XRD, and field-emission scanning electron microscopy (EF-SEM).

2. Experiment

Thin films of A15 W were grown on Si(100) and/or NaCl substrates at room temperature in a deposition chamber with a base pressure of $\sim 5 \times 10^{-6}$ Torr by dc magnetron sputtering. A 50 mm diameter tungsten cathode was sputtered with a power of 90 W at an Ar sputtering pressure varying in the range of 5–25 mTorr. Prior to deposition, the target was sputter cleaned for 5 min while the substrates were isolated from the plasma by a shutter. All films were deposited to a nominal thickness of 50 ± 5 nm. Using TEM and XRD it was found that the A15 W phase was irreversibly transformed to a stable bcc W structure after a thickness of ~100–120 nm was reached in the pressure range of 5–12 mTorr, in agreement with previous studies [1–5]. At higher pressures (>20 mTorr), the transformation was not observed up to ~250 nm.

Elemental chemical-state information and concentration were obtained using XPS. The measurements were performed in a Kratos Axis/800 hemispherical energy analyzer equipped with an unmonochromatized Mg Kα x-ray source ($h_\nu = 1253.6$ eV). The binding

* Author to whom all correspondence should be addressed.

0022–2461 © *2001 Kluwer Academic Publishers*

energy scale was calibrated using Ag and Au standards. Surface impurities such as carbon were also used as internal references. Oxygen impurities were also analyzed by collecting O K-edge loss spectra using EELS. Film phase transition was characterized using a Siemens D5000 diffractometer operated at 40 kV and 30 mA. The measurements were carried out using Cu Kα radiation with a Ni filter to remove Cu Kβ reflections. Film morphology was also investigated using FESEM (JEOL JSM-6000) operated at 15 kV.

Transmission electron diffraction patterns were acquired in a Phillips EM430 instrument fitted with a GATAN 666 parallel electron energy-loss system operating at 300 kV, as described in earlier papers [16, 17]. Briefly, the electrons passed through a post-column magnetic spectrometer and the elastically scattered electrons were selected using an energy window of about 2 eV in width centred on zero energy-loss peak. The electron intensity was sequentially recorded under computer control as a function of the reciprocal space coordinate by shifting the diffraction pattern across the entrance aperture of the spectrometer. The background subtraction was performed using the tabulated electron scattering factors [18].

3. Theory

Structure in an A15 W material is essentially of a long-range nature and is best described by RDF, which gives a measure of nearest neighbour distances between atoms. The RDF, denoted $G(r)$, is calculated as Fourier sine transformation of the electron diffraction intensities $I(q)$ in real space:

$$4\pi r[\rho(r) - \rho_0] = 8\pi \int_0^\infty \frac{q[I(q) - b^2]}{b^2} W(q) \sin 2\pi rq \, \mathrm{d}q \quad (1)$$

where ρ_0 is the average atomic density, $\rho(r)$ is the atomic density at a distance r from a given atom at the origin, and b is the coherent scattering length of tungsten. The Lorch window function $W(q) = \sin(\pi q/q_{\max})/(\pi q/q_{\max})$ was used in the determination of the RDF's. The scattering factor $q = 2\sin\theta/\lambda$ was collected to a maximum value of q, $q_{\max}$, of 3.5 Å^{-1}.

The theoretical $G(r)$ were calculated from the diffraction intensities $I(q)$ determined using the Debye scattering equation

$$I(q) = \sum_{m=1}^{N} \sum_{n=1}^{N} f_m f_n \frac{\sin 2\pi q r_{mn}}{2\pi q r_{mn}} \quad (2)$$

for an array of N atoms which takes all orientations in space and r_{mn} is the distance between atoms m and n. The calculated $I(q)$ was truncated to the same range of q as the experimental data, then Fourier sine transformed to produce a $G(r)$.

In order to quantitatively assess the best fit between data and simulations, a reliability R-factor analysis is used [19, 20].

$$R = \frac{1}{K} \left\{ \sum_{i=1}^{K} \left[\frac{G_{\mathrm{EXP}}(r) - G_{\mathrm{MODEL}}(r)}{G_{\mathrm{EXP}}(r)} \right]^2 \right\}^{\frac{1}{2}} \quad (3)$$

where $G_{\mathrm{EXP}}(r)$ and $G_{\mathrm{MODEL}}(r)$ are the experimental and calculated $G(r)$ distributions, respectively, and K is the number of experimental data points.

4. Results

4.1. Oxygen impurities by XPS and EELS

An increase in the oxygen concentration of A15 W films with increasing Ar sputtering pressure is shown in Fig. 1. The data were derived from a series of A15 W films using both XPS and EELS. The points labelled A and B gave the XPS W 4f and O 1s and EELS O K-edge spectra shown, respectively. Uncertainties of the data were estimated to be ±10% by XPS and ±15% by EELS. The XPS results show that the A15 W films contained 5–12 at. % oxygen at Ar sputtering pressure range of 5–25 mTorr, while the EELS analysis indicates 6–15 at. % oxygen, respectively. These values were obtained based on repeated measurements involving

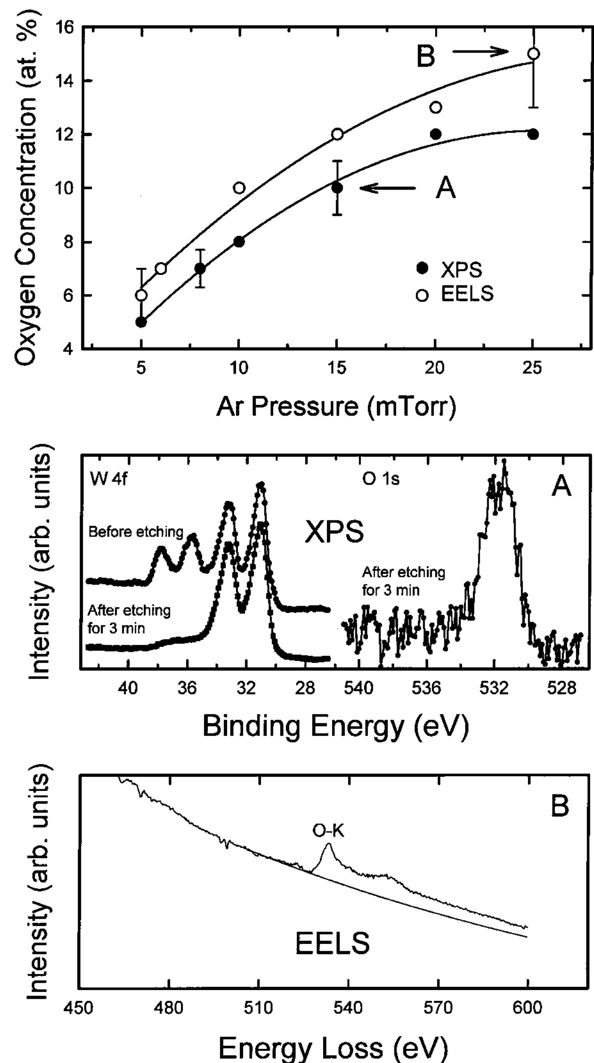

Figure 1 Oxygen atomic concentration in the A15 films determined by both XPS and EELS as a function of Ar sputtering pressure. Typical XPS W 4f and O 1s and EELS O K-edge spectra labelled A and B, respectively, are also shown.

many freshly deposited samples over many weeks. The good agreement between the oxygen impurities obtained from two independent techniques lends confidence to the oxygen concentration value and the reliability of the experimental data. The oxygen content became slightly less for higher film thickness.

Close examination of the deposition processing reveals that the most likely source of oxygen contamination was either from residual oxygen in the deposition chamber or from the tungsten sputter target under the present experimental conditions. The difference in oxygen concentration was mainly controlled by the deposition rate, i.e. competitive effect between the tungsten deposition rate and the contamination incorporation rate. The longer the sputtering time, the lower the oxygen content in the film.

4.2. Stacking faulted structure by EFED

Fig. 2b shows the EFED $I(q)$ pattern in the momentum space as a function of the scattering factor q obtained from an A15 W film containing ~15 at. % oxygen (measured by EELS). The angular scale of the diffraction pattern and its centre were calibrated by indexing the diffraction pattern of a known standard of polycrystalline aluminium [see Fig. 2a]. The $I(q)$ pattern for the A15 W film in Fig. 2b shows the polycrystalline long-range order features. The characteristics of the patterns agree with observations obtained by TEM. All the lines (hkl) corresponding to the A15 phase are clearly detected. It is interesting to note that some forbidden reflection peaks, such as (100)* at $q \approx 0.20$ Å^{-1} and (110)* at $q \approx 0.28$ Å^{-1}, are observed, indicating the existence of ordered substitutional or interstitional lattice defects in the A15 W structure. The forbidden reflection peaks (220)* and (300)* also appear in the $I(q)$ pattern, although they are not resolved. These observations are in good agreement with previous studies by several research groups using TED [10–15]. These authors, however, discuss only the stacking faults formed in the A15 W films without further justification.

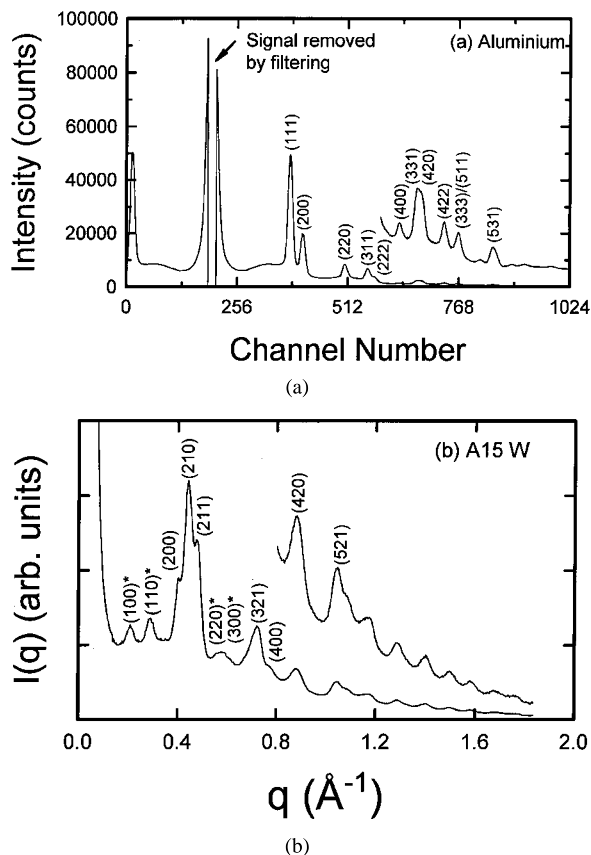

Figure 2 Experimentally measured electron diffraction intensities (a) from the polycrystalline aluminium film for Miller index calibration and (b) from the A15 W film deposited at ~25 mTorr. Note that intensities in (a) for exceeding a maximum permissible count of $2^{14} - 1$ were removed by filtering (total 20 channels).

In order to obtain detailed structural information, the most effective and direct method is to compare the experimental $G(r)$ with the corresponding theoretical calculations because a relationship in the coordinate space can be interpreted much easier than the correlation in the momentum space. Successive peaks in $G(r)$ correspond to first-, second-, and higher-order nearest neighbour atomic distances.

A major question concerning A15 W is whether it is an ordered W_3W phase or a stacking faulted W_3W structure or a mixture of both two. There are two different atomic positions in the A15 (A_3B) structure [21], six A positions with two nearest neighbours at a distance of 2.52 Å and two B positions with twelve nearest neighbours at a distance of 2.82 Å. The initial stacking sequence for A15 is ABCBABCB (Layers A, B, C, and B are spaced by 1/4 a, the lattice parameter of the A15 structure). The observation of the forbidden reflections in an electron diffraction pattern restricts any structural models to the different stacking of A15 layers. We consider three possible stacking faulted sequences: ABBCABBC, ACBBACBB, and ABABABAB, respectively. It is noted that the ABABABAB stacking is a twin-related W_3W structure. Close examination reveals that the nearest neighbour W-W distance of 1.78 Å in both ABBCABBC and ACBBACBB stacking structures cannot be true because the diameter of a tungsten atom is 2.52 Å. Therefore, these two models can be excluded. On the basis of the above considerations as well as possible phase formation induced by oxygen impurities, five possible models for the A15 structure can be proposed: (i) model A: an ordered W_3W structure, i.e. normal ABCBABCB stacking; (ii) model B: a stacking faulted ABABABAB structure, (iii) model C: a 50% mixture of both (i) and (ii), (iv) model D: a random distributed $W_{85}O_{15}$ structure, and (v) model E: a W_3O phase.

Fig. 3 compares the experimental $G(r)$ obtained by Fourier sine transformation of $I(q)$ in Fig. 2b with five calculated models. Based on the observed and calculated features in $G(r)$, the following characteristics can be discussed: (i) The experimental $G(r)$ shows a broader first peak centred at 2.92 Å, due to the existence of three peaks corresponding to the first, second, and third nearest neighbours ($r_1 = 2.52$, $r_2 = 2.82$, and $r_3 = 3.08$ Å, respectively). (ii) The calculated $G(r)$ for model A has almost the same peak positions, shape and amplitudes of the experimental observed peaks, however, it fails to predict the peak at 3.80 Å. The model B provides a feature at 3.76 Å, however, its amplitude is

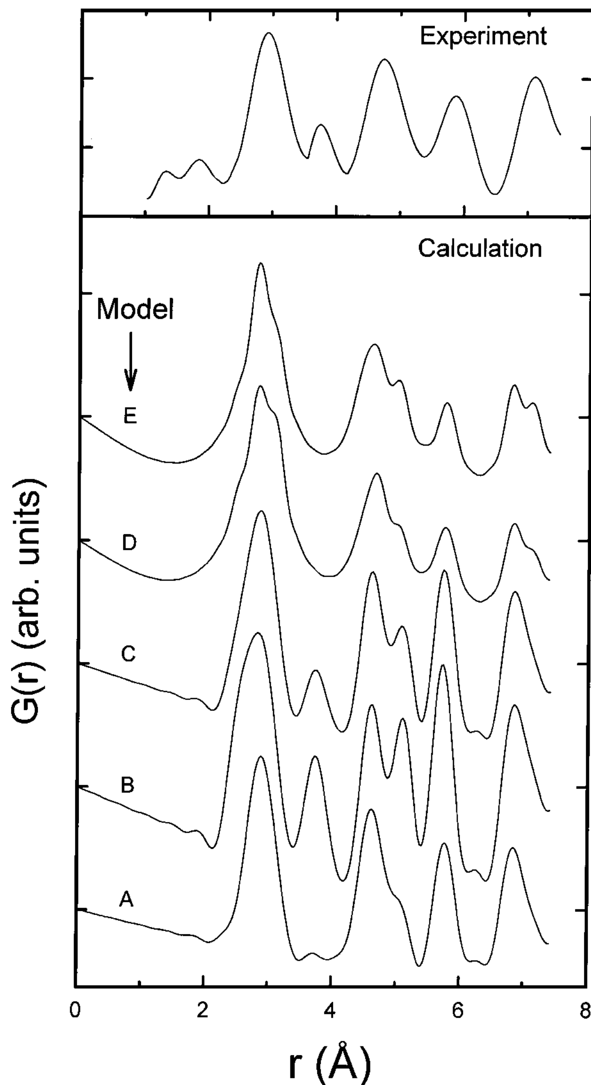

Figure 3 Experimentally determined and theoretically calculated $G(r)$ for five structural models are compared. Simulations were performed with 128 atoms for models A, B and C and 64 atoms for models D and E, respectively, with periodic boundary conditions. The simulated $G(r)$ curves have been normalized to the first peak height.

too higher. In addition, for the model B the first peak is broader and the third peak splits into two peaks, contrast to the experimental observations. (iii) The models D and E also fail to produce the peak at 3.80 Å. We conclude that the peak at 3.80 Å is attributed to the existence of ordered substitutional or interstitional lattice defects in the A15 W structure. (iv) Features in the low-r region (<2.0 Å) for the experimental $G(r)$ are the least reliable because they are most strongly affected by the small-angle inelastic scattering effect associated with a considerable fraction of small voids. (v) An O-O coordination cannot be observed by both experiment and calculation (models D and E) because of its very small scattering power compared to tungsten and the small weighting factor in the composition range.

The agreement between the experimental and simulated $G(r)$ was judged on the basis of the reliability R-factor using Equation 3. R factors were calculated for comparison of each of the simulated $G(r)$ curves with the experimental data in the range of 2.0–7.5 Å (Fig. 3). The result of the R-factor analysis is shown in

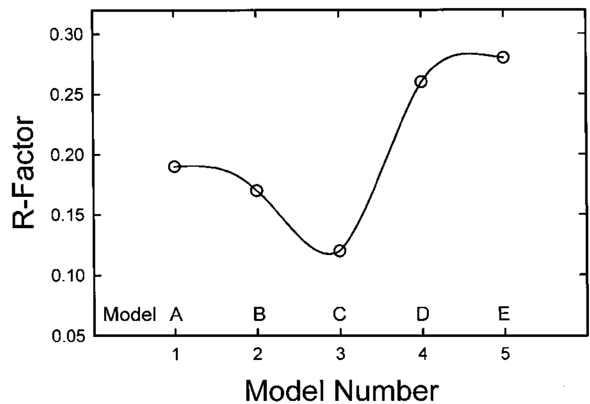

Figure 4 Plot of the R factor versus the model number for comparison of the experimental and simulated $G(r)$ curves of Fig. 3.

Fig. 4, where the R factors are plotted as a function of the model number. The best fit to the experimental $G(r)$ was achieved with the minimum R-factor of $R = 0.12$ for the model C. This mixed model of ordered and stacking faulted W_3W structures provides the best fit to all of the features, which is a good reproduction of the experimental $G(r)$. In the simulations, the relative percentages of model A and model B structures were not varied. This is direct evidence for the presence of mixed ordered and stacking faulted W_3W structures with approximately equal abundance. Repeated measurements involved more than five freshly prepared A15 W samples in Ar sputtering pressure range of 5–25 mTorr over several weeks showed that the minimum in R factors was reproducible to within $\pm 15\%$.

We would like to point out that differences between model C and experiment can also be clearly seen. The third peak at ∼4.7 Å from the calculation has a small shoulder at ∼5.1 Å and the fifth peak at substantially lower value (∼6.9 Å) than the experimental one (∼7.1 Å). We explain that such discrepancy is related to stacking faults and localized disorder in the grain boundaries, leading to deviation from the perfect structure.

4.3. Anneal effect

The A15 W phase is metastable because it transforms to the stable bcc W by anneal. However, in many cases many researchers have misinterpreted the origin of this transformation as a stress effect or a critical thickness induced transformation. To understand the role of oxygen in forming and stabilizing the A15 W structure, three independent measurements were carried out using EELS, TED, and XRD analysis. The results of EELS analysis by *in situ* anneal from an A15 film are shown in Fig. 5, in which the oxygen concentrations are plotted as a function of film temperature. The points labelled A and B gave the O K-edge EELS spectra shown. The corresponding XRD patterns (also labelled A and B) recorded from the original A15 W film (the film was deposited on a Si(100) substrate simultaneously) and after transforming to the bcc are also shown. The results indicate that with increasing temperature the oxygen atoms move increasing outward. The A15 W phase

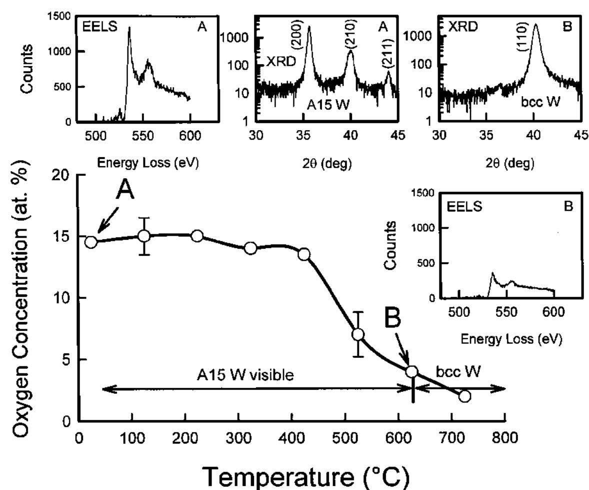

Figure 5 Oxygen concentration as a function of film temperature by EELS. Error bars are based on 4–6 measurements. From each point, data were taken during *in situ* heating at 20 °C min^{-1}, held for 5 min and then the O K-edge spectrum was taken. The EELS spectra and corresponding XRD patterns labelled A and B recorded from the original and after the phase transformation are also shown. The film was prepared at an Ar pressure of ~25 mTorr.

is completely transformed to the bcc W structure by annealing to ~625 °C. The most interesting feature for this observation is that the phase transformation from A15 to bcc by higher temperature annealing was accompanied by reduction of oxygen in the films. These results have not been previously published and further support the role of oxygen in forming and sabilizing the A15 W structure. This direct evidence leads one to believe that the A15 phase is stabilized by a small amount of oxygen without forming a W_3O compound. We can suggest that the transformation from A15 W to bcc W is thermally activated requiring higher temperature to cause the oxygen impurities to outdiffuse (segregate to the surface) and to bring about the long-range ordering, and then to transit to the stable bcc structure. We would also like to point out that, once a bcc W phase was prepared, the reverse transformation has never been observed.

Our FESEM measurements also indicate that a significant increase of the tungsten particles was observed after the phase transformation from A15 W to bcc W. In the as-deposited condition the A15 particle size was on the order of 5–10 nm [Fig. 6a], but after transformation the particle size was much larger, approaching ~25–30 nm in diameter [Fig. 6b]. Another interesting observation is the existence of conglomerates of columns for the A15 film. Such conglomerates may comprise some tens to some hundreds of individual columns. After anneal treatment, the columnar microstructure has been preserved.

5. Discussion

The results of the present investigation have shown that energy-filtered electron diffraction in a combination with XPS, EELS, and XRD is a powerful technique, which is capable of determining oxygen impurities, detecting the stacking faulted A15 W structure and producing quantitative data of the atomic distance

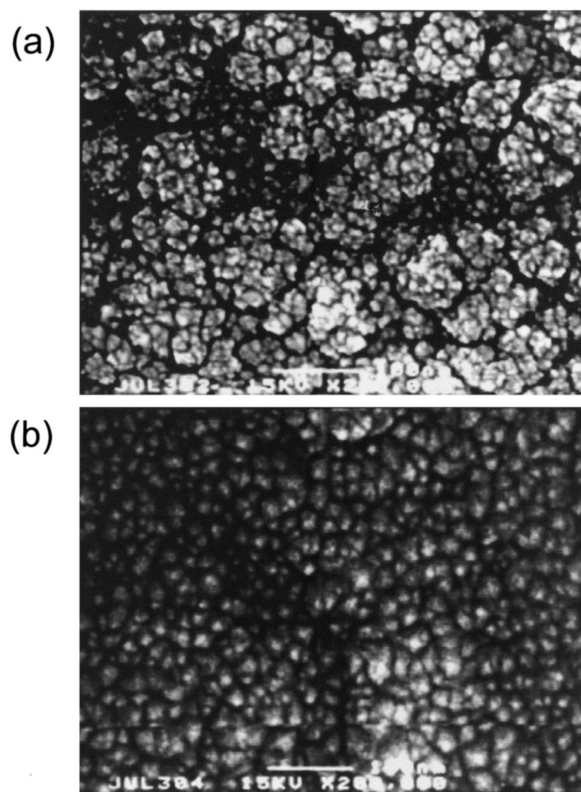

Figure 6 FESEM micrographs of: (a) an as-deposited A15 W film and (b) the same film after complete transformation into bcc W by annealing. The film was prepared at ~20 mTorr and annealed to 650 °C for 30 min in a vacuum of ~2×10^{-7} Torr.

parameters. TED images reported by many research groups reveal that the A15 W phase is not a perfect A15 structure because kinematically forbidden reflections are observed. However, its exact structure remains unknown due to large uncertainties involved in diffraction and spectroscopic measurements. In this study the particular model was chosen because its simulated $G(r)$ curve (model C) provides better agreement with the experimental $G(r)$ curve than any of other models used. Good correspondence between the observed and calculated $G(r)$ distributions indicates that the A15 W is composed of ordered and stacking faulted W_3W structures.

Because of a small amount of oxygen (about 5–12 at. % by XPS and 6–15 at. % by EELS in the 50-nm-thick films) observed in the films as well as its very small scattering power compared to tungsten, oxygen was not observed directly in the experimental $G(r)$ curves. However, it may have effects on the arrangements of heavier tungsten atom bonded to lighter oxygen. The effects on the bond distances are expected to be negligible, but the peak heights may be affected owing to the variations in W-W, O-O, and W-O coordination. We are currently examining this effect and related experimental questions.

There are three major experimental observations, which are related to the stability of the A15 W phase by the presence of oxygen under the current experimental conditions. First, the A15 W phase is induced by a small amount of oxygen without forming a W_3O compound. Second, by FESEM the A15 W sample has a very column microstructure with a finer grain structure. This

can be explained in terms of oxygen enrichment at the column boundaries, thus preventing further growth and promoting fine grains. Third, as examined by EELS and XRD, temperatures as high as ∼550–650 °C (depending on the Ar gas pressure) were required to induce the phase transformation from A15 W to bcc W in the films investigated. The higher the oxygen concentration in the film, the higher the transformation temperature required. We conclude that thermally induced phase transformation may serve to stabilize the stable bcc structure, although the dynamics of the structure transformation are not known in detail. Based on the results obtained and the above discussion, the phase transformation from A15 W to bcc W in the film is believed to be governed by two main trends: (i) From an energetic point of view, the stacking faulted energy required to stabilize the A15 W structure must be overcome in order for transformation to occur. (ii) From a structural point of view, the transformation to bcc W occurs by dissolution of the stacking faults and localized rearrangement of the lattice. No long range diffusion or atomic movement is required.

In examining the tungsten related phase diagram we have not been able to identify a unique bulk phase, which could fully account for the observed A15 W structure. In light of this, we envision that the A15 W phase is not characteristic of any bulk compound and therefore seems to be uniquely associated with the presence of incorporated oxygen. The exact mechanism for the formation of the metastable phase stabilized by oxygen impurities is not clear. Further study with ab initio total-energy calculations for establishing the origin of the A15 W phase induced by a small amount of oxygen is in progress in our Materials Research Centre. The fact that the A15 W phase appears over such a range of oxygen concentrations may be due to the fact that it is kinetically prevented from converting to thermodynamically favorable phase, bcc W, or that a very dilute bulk oxygen composition might be sufficient to completely stabilize the A15 W structure.

6. Conclusion

The oxygen-induced A15 W structure (50 nm in thickness) prepared by magnetron sputtering was experimentally determined for the first time using energy-filtered electron diffraction in a combination with XPS, EELS, FESEM, and XRD. The reduced density function $G(r)$ calculated by Fourier sine transformation from the transmission electron diffraction intensities collected from the A15 W films was compared to theoretical calculations based on several possible structural models. By using a reliability R-factor analysis the A15 W structure has been determined. The mixed phase consisting of ordered and stacking faulted W_3W structures showed good correspondence between the observed and calculated $G(r)$ distributions, indicating that forbidden reflections in some of the diffraction patterns provided direct evidence of a fault-stabilized crystal structure. The role of oxygen impurities in forming and stabilizing the A15 W structure was also elucidated by *in situ* anneal in the TEM and EELS system.

The results have at least two general implications. The first concerns the nature of the interaction of oxygen impurities and tungsten films. The second implication is related to a general principle of governing the formation and stability of a stacking faulted metastable phase induced by impurity incorporation during film growth.

Acknowledgements

The authors gratefully acknowledge the financial support of this work by the Australian Research Grants Scheme. The authors also appreciate the use of the facilities in the Australian Key Centre for Microscopy and Microanalysis, University of Sydney, which is supported by Australia Research Council.

References

1. I. A. WEERASEKERA, S. I. SHAH, D. V. BAXTER and K. M. UNRUH, *Appl. Phys. Lett.* **64** (1994) 3231.
2. M. S. AOUADI, R. R. PARSONS, P. C. WONG and K. A. R. MITCHELL, *J. Vac. Sci. Technol. A* **10** (1992) 273.
3. J. H. SOUK, J. F. O'HANLON and J. ANGILLELO, *ibid.* **3** (1985) 2289.
4. A. J. LEARN and D. W. FOSTER, *J. Appl. Phys.* **58** (1985) 2001.
5. E. K. BROADBENT, *J. Vac. Sci. Technol. B* **5** (1987) 1661.
6. Y. PAULEAU, PH. LAMI, A. TISSIER, R. PANTEL and J. C. OBERLIN, *Thin Solid Films* **143** (1986) 259.
7. A. BENSOULA, J. C. WOLFE, A. IGNATIEV, F. O. FOND and T. S. LEUNG, *J. Vac. Sci. Technol. A* **2** (1984) 389.
8. A. M. HAGHIRI-GOSNET, F. R. LADAN, C. MAYEUX and H. LAUNOIS, *Appl. Surf. Sci.* **38** (1989) 295; *ibid. A* **7** (1989) 2663.
9. H. S. WITHAM, P. CHINDANDOM, I. AN, R. W. COLLINS, R. MESSIER and K. VEDAM, *ibid.* **11** (1993) 1881.
10. P. PETROFF, T. T. SHENG, A. K. SINHA, G. A. ROZGONYI and F. B. ALEXANDER, *J. Appl. Phys.* **44** (1973) 2545.
11. M. J. O'KEEFE, J. T. GRANT and J. S. SOLOMON, *J. Electron. Mater.* **24** (1995) 961.
12. M. ARITA and I. NISHIDA, *Surf. Rev. Lett.* **3** (1996) 1191.
13. T. KIZUKA, T. SAKAMOTO and N. TANAKA, *J. Cryst. Growth* **131** (1993) 439.
14. D. P. BASILE, C. L. BAUER, S. MAHAJAN, A. G. MILNES, T. E. JACKSON and J. DEGELORMO, *Mater. Sci. Eng. B* **10** (1991) 171.
15. M. J. O'KEEFE and J. T. GRANT, *J. Appl. Phys.* **79** (1996) 9134.
16. D. R. MCKENZIE, D. A. MULLER and B. A. PAILTHORPE, *Phys. Rev. Lett.* **67** (1991) 773.
17. D. J. H. COCKAYNE and D. R. MCKENZIE, *Acta. Crystallogr.* **44** (1988) 870.
18. International Tables for Crystallography, Vol. C, edited by A. J. C. Wilson (Kluwer Academic Publisher, the Netherlands, 1995).
19. Y. G. SHEN, J. YAO, D. J. O'CONNOR, B. V. KING and R. J. MACDONALD, *Phys. Rev. B* **56** (1997) 9894.
20. Y. G. SHEN, A. QAYYUM, O'CONNOR and B. V. KING, *ibid.* **58** (1998) 10025.
21. ASM Metals Reference Book, edited by M. Bauccio (American Society for Metals, Metals Park, OH, 1994).

Received 9 November 1999
and accepted 10 April 2000